PLANT SCIENCES

Establishing a reproducible approach to study cellular functions of plant cells with 3D bioprinting

Lisa Van den Broeck[1], Michael F. Schwartz[1]†, Srikumar Krishnamoorthy[1]†, Maimouna Abderamane Tahir[1,2]†, Ryan J. Spurney[1,3], Imani Madison[1], Charles Melvin[1], Mariah Gobble[1], Thomas Nguyen[1], Rachel Peters[1], Aitch Hunt[1], Atiyya Muhammad[1], Baochun Li[4], Maarten Stuiver[5], Timothy Horn[2]*, Rosangela Sozzani[1]*

Capturing cell-to-cell signals in a three-dimensional (3D) environment is key to studying cellular functions. A major challenge in the current culturing methods is the lack of accurately capturing multicellular 3D environments. In this study, we established a framework for 3D bioprinting plant cells to study cell viability, cell division, and cell identity. We established long-term cell viability for bioprinted Arabidopsis and soybean cells. To analyze the generated large image datasets, we developed a high-throughput image analysis pipeline. Furthermore, we showed the cell cycle reentry of bioprinted cells for which the timing coincides with the induction of core cell cycle genes and regeneration-related genes, ultimately leading to microcallus formation. Last, the identity of bioprinted Arabidopsis root cells expressing endodermal markers was maintained for longer periods. The framework established here paves the way for a general use of 3D bioprinting for studying cellular reprogramming and cell cycle reentry toward tissue regeneration.

INTRODUCTION

A tight coordination between cellular reprogramming, i.e., the dedifferentiation of cells into a pluripotent state, and cell cycle progression via cell-to-cell communication is required for tissue regeneration. For plant and animal cells, cell-to-cell communication is affected by mechanical and positional cues as a result of the physical and molecular interaction between cells and their microenvironment (*1*, *2*). Alterations in cell-to-cell communication due to a changing microenvironment can adjust cellular behavior and trigger cellular reprogramming. Thus, recapitulating the multicellular three-dimensional (3D) microenvironment behind cell-to-cell and cell-to-environment communication is key to gaining insights into the mechanical and positional context that governs cellular reprogramming toward tissue regeneration.

Multiple studies have established that conventional cell culturing methods do not entirely mimic the 3D microenvironment observed under natural conditions (*2*, *3*). 3D bioprinting enables the generation of specifically designed 3D cellular constructs that better simulate natural in planta conditions (*4*). 3D bioprinting can be performed through the application of one or multiple modalities for the precise spatial deposition of biologically active material, referred to as a bioink. To enable the spatial deposition of cells and simultaneously provide structural support, plant cells can be immobilized and bioprinted within a plethora of hydrogel scaffolds (*5*). As such, 3D bioprinting provides an amenable and controllable system to fabricate complex systems that capture cellular dynamics and interactions in a physiologically accurate manner toward tissue regeneration (*6*–*9*). For example, human induced pluripotent stem cells have been bioprinted to study cell fate, phenotypic variation, and tissue regeneration (*7*). Plants inherently show extreme regenerative capacities. For example, the complete loss of the root stem cells can be fully replaced and functional within hours (*10*). The regenerative capacities of individually isolated plant cells are greatly affected by cell type, tissue type, genotype, and the specific 3D microenvironment (*1*). Thus, to design and engineer 3D microenvironments that consistently reproduce a cellular response, genotype-specific and cell type–specific designs are needed (*11*). For such designs, mechanical properties, nutrient supply, degradability, and tissue mimicry need to be considered (*11*). With 3D bioprinting, the mechanical and positional cues can be controlled by depositing living plant cells in a well-defined environment. In addition, to achieve a reproducible cellular response, bioprinting metrics should be considered, including construct dimensions, cell density, speed and pressure during extrusion, and nozzle diameter.

Here, we used Arabidopsis root–derived protoplasts, i.e., plant cells without cell wall, as a model system to showcase the potential of 3D bioprinting to study cell viability, cell division, and cellular reprogramming in a tunable microenvironment. Protoplasts are an alternative system to callus and suspension cultures that exhibit individual cellular behavior. Specifically, we maintained bioprinted Arabidopsis root cells isolated from two different tissue types for up to 7 days. In this time frame, we showed that the percentage of isolated cells expressing endodermal markers increases, indicating that the identity of isolated cells changes over longer periods of time. Supportively, gene expression profiling showed an induction of stem cell lineage markers and regeneration-related genes, suggesting that the bioprinted cells gain a stem cell–like identity. Last, we demonstrated the applicability of 3D bioprinting for studying regeneration of isolated single cells for model and crop species.

RESULTS

Demonstrating the maintenance of 3D bioprinted Arabidopsis root cells

Cellular functions such as cell differentiation, cell cycle progression, responsiveness to stimuli, and cellular reprogramming are driven

[1]Plant and Microbial Biology Department, North Carolina State University, Raleigh, NC 27695, USA. [2]Mechanical and Aerospace Engineering Department, North Carolina State University, Raleigh, NC 27695, USA. [3]Electrical and Computer Engineering Department, North Carolina State University, Raleigh, NC 27695, USA. [4]Innovation Center of BASF, Morrisville, NC 27560, USA. [5]BASF Innovation Center, Technologiepark 101, 9052 Zwijnaarde, Belgium.
*Corresponding author. Email: ross_sozzani@ncsu.edu (R.S.); tjhorn@ncsu.edu (T.H.)
†These authors contributed equally to this work.

by cell-to-cell and cell-to-environment communication. These cell-to-cell and cell-to-environment signals are not entirely captured in suspension cell cultures due to the lack of a natural microenvironment (*12*–*14*). On the other hand, 3D encapsulation methods can replicate the natural microenvironment. Moreover, they can immobilize plant cells, allowing for more physiologically accurate cellular behavior. We used 3D bioprinting to recapitulate the plant cells' microenvironment and behavior. For this, we optimized two key aspects of successful bioprinting, which include the bioink and bioprinting parameters. The bioink is a combination of living cells and the scaffold material that provides support to the cells and the nutrients needed to ensure cell viability (*15*). To achieve long-term cell viability, we optimized tissue-specific bioinks and established a reproducible experimental pipeline that consists of bioprinting protoplasts and maintaining and imaging the bioprinted constructs over time (Fig. 1A). In this pipeline, we focused on *Arabidopsis thaliana* roots, a tissue of which the maintenance outside its context is known to be technically challenging (*16*). In addition, to further gain insights into whether different tissue types would be more prone to cellular reprogramming, we isolated protoplasts from both meristematic and differentiated root tissue and performed comparative analyses. These comparative analyses and time course experiments resulted in large-scale image datasets. To process and analyze these large image datasets generated from our bioprinting pipeline, we developed a semiautomated and high-throughput image analysis pipeline that can quantify cells in confocal z-stack images (see Materials and Methods). To make it freely available for the scientific community, the entire pipeline was wrapped in a graphical user interface (GUI) (https://github.com/LisaVdB/Confocal-z-stack-cell-detection and 10.5281/zenodo.7012765) (Fig. 1B).

Tissue-specific bioinks require the balancing of auxin and cytokinin, which are critical for long-term cell viability and proliferation (*1*). In addition, several other compounds have been identified to activate the intrinsic cellular programs that trigger cell division. To establish a reproducible pipeline using plant cells for 3D bioprinting that supports viable cells for extended periods, we used optimized concentrations of auxin and cytokinin and added phytosulfokine (PSK) and folic acid, two compounds that stimulate cell proliferation, to the bioink (see Materials and Methods) (*17*–*19*). In addition, to avoid the formation of a thermal gradient within the bioink and our cells, we incorporated an axial piston in the cartridge. After optimization, a usual experiment yielded 62.2 ± 8.2% and 51.6 ± 8.3% viable meristematic and differentiated protoplasts immediately (day 0) after 3D bioprinting. After 5 days, generally 27.7 ± 7.6% and 29.5 ± 3.5% of the meristematic and differentiated isolated cells were still viable (Fig. 1C; fig. S1, A and B; and data S1). When stained with propidium iodide, a contrast staining for cell death, similar cell viability percentages were obtained (fig. S1, C to E). Thus, we opted to use bright field to assess cell viability so that we could use the red channel to quantify cell marker expression of, for example, pSCR:SCR-mCherry (pSCARECROW:SCARECROW-mCherry). Given that, after bioprinting, 40% of the root protoplasts were not viable, we compared the viability of bioprinted cells to manually pipetted cells. Manually pipetted meristematic and differentiated protoplasts showed a slightly reduced but comparable viability to bioprinted cells of 44.9 ± 6.6% and 48.6 ± 6.6%, respectively. These results indicate that the bioprinting process has no observable detrimental effect on cell viability but rather the protoplast isolation (Fig. 1D and data S1).

3D bioprinting requires a suitable scaffold that is biocompatible, ensures transfer of nutrients and oxygen to the cells, and offers structural support (*20*). As scaffold in our experimental pipeline, we chose low melting agarose because of its established biocompatibility and thermal cross-linking properties that facilitate the operational workflow (*20*). However, it was previously reported that Arabidopsis shoot cells encapsulated in sodium alginate were viable and able to regenerate (*21*, *22*). To test the compatibility of sodium alginate with bioprinting Arabidopsis root cells, we bioprinted protoplasts in two different scaffolds, namely, 0.6% (w/v) low melting agarose and 0.75% (w/v) sodium alginate (*21*, *22*). After 5 days, we observed 23.6 ± 5.8% viability within the agarose compared to 7.7 ± 1.3% with the sodium alginate (Fig. 1E and data S1), and after 7 days, we observed mechanical deformations in the alginate constructs in some cases (fig. S1F). We reasoned that this was due to excess swelling as a result of the short cross-linking treatment, knowing that the duration of cross-linking directly determines the stiffness and thus the swelling of the bioprinted constructs (*23*, *24*). In addition, posttreatment cross-linking due to the calcium ions in our bioink could affect the swelling (*25*). Therefore, we chose to primarily use low melting agarose as the scaffold material in this study.

Overall, we demonstrated the utilization of extrusion-based 3D bioprinting to reliably deposit plant cells isolated from different tissue types and demonstrated the possibility of using different scaffold materials in the bioprinting process. We showed the maintenance of Arabidopsis root protoplasts within 3D bioprinted constructs for 5 days while maintaining a viability of more than 25%.

Applicability of 3D bioprinting toward plant cell regeneration

Bioprinting isolated cells into designed cellular constructs provides a system to evaluate cellular regeneration. Previous studies have shown that cellular regeneration by callus formation from root explants initiates with divisions of pericycle cells, rather than dedifferentiation and cell cycle reentry of root cells (*22*). To our knowledge, cell cycle reentry of protoplasts derived from Arabidopsis roots has not yet been achieved (*16*, *22*). To understand whether bioprinted root cells can reenter the cell cycle, we evaluated divisions and microcallus formation. We observed that bioprinted Arabidopsis root cells undergo their first cell division as early as 3 days (Fig. 2, A and B). To map the cells' potential to divide, we used the cell cycle marker pCYCB1;1:CYCB1;1-GFP, which is expressed at the transition from the G2 gap phase into mitosis (M phase) (fig. S2) (*26*). Over the evaluated time course, on average, ~5 and ~2% of the bioprinted meristematic and differentiated root cells expressed CYCB1;1, respectively, indicating the restricted potential of protoplasts to reenter the cell cycle (Fig. 2C and data S1). After a 7- to 10-day period, ~12% of the bioprinted constructs developed a microcallus, here defined as four cells or more (Fig. 2B and data S2). To investigate the cellular reprogramming underlying the initial cell divisions before microcallus formation, we collected RNA from isolated differentiated root cells on days 0, 1, and 3 after bioprinting. Pairwise comparisons at each time point revealed 9071 differentially expressed genes (DEGs) ($q \leq 0.05$, $|\text{fold change}| \geq 2$) (fig. S3, A to D, and data S3). We identified seven clusters of coexpressed genes, and Gene Ontology (GO) enrichment analysis showed different biological processes for these clusters (fig. S3, A and B). Cluster 1 contained genes related to cell division and were up-regulated at day 3 (fig. S3B). Specifically, in the analyzed time frame, several core cell

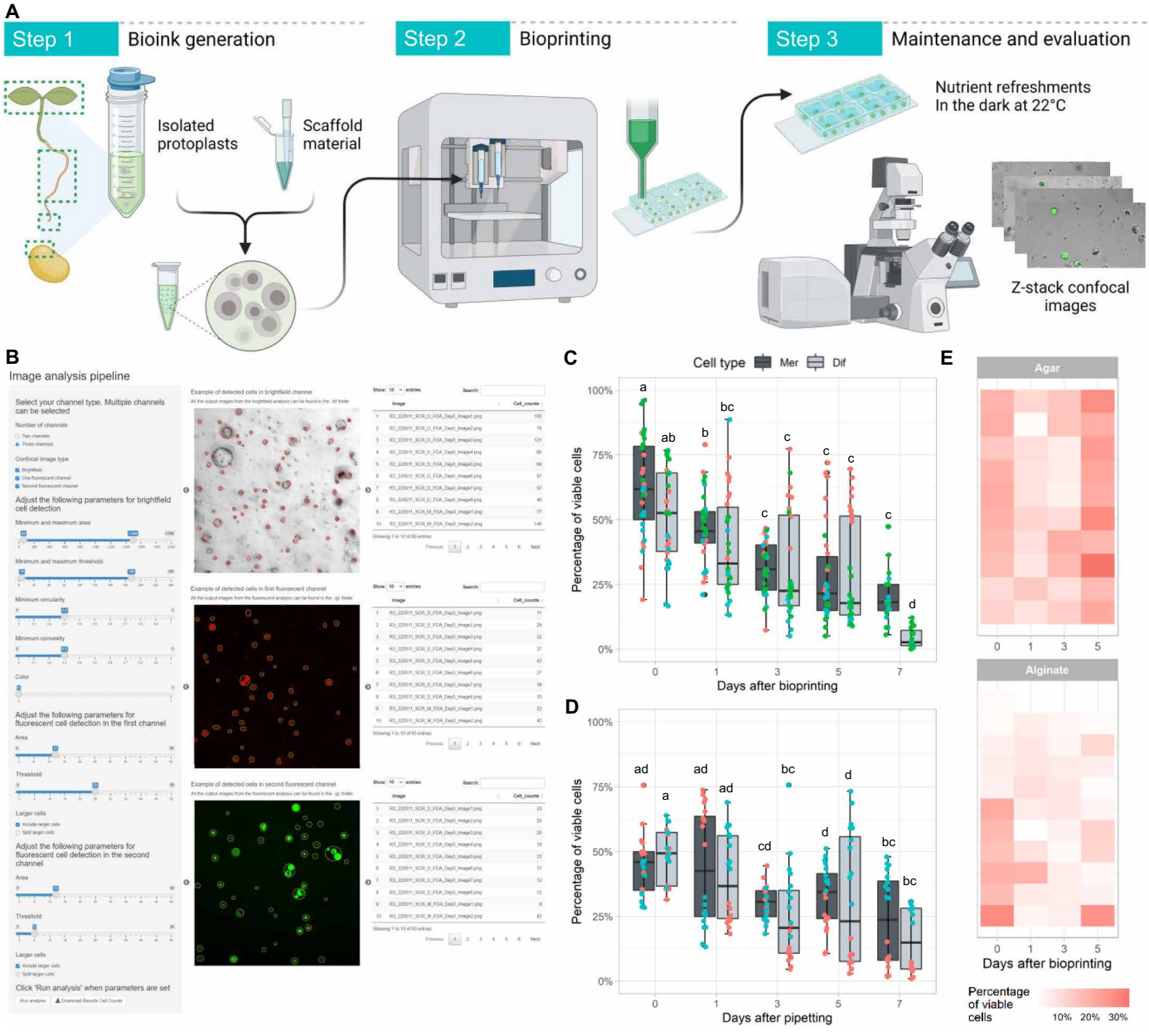

Fig. 1. Maintenance of bioprinted Arabidopsis root cells. (**A**) Schematic overview of the key steps in our 3D bioprinting protocol (created with BioRender.com). Step 1: Combining protoplasts and scaffold material to generate bioink. Step 2: 3D bioprinting. Step 3: Maintaining and imaging over time. (**B**) Screenshot of the graphical user interface (GUI) of our analysis pipeline for high-throughput quantification of cells in confocal z-stack images. (**C** and **D**) Percentage of viable cells isolated from meristematic (Mer) and differentiated (Dif) root tissue upon 3D bioprinting (C) or manual deposition (D). (**E**) Percentage of viable cells upon bioprinting with two different scaffolds: 0.6% low melting agarose and 0.75% sodium alginate. Cell viability was evaluated with fluorescein diacetate staining immediately after bioprinting (day 0) and on days 1, 3, 5, and 7. Colored dots on box plots represent the independent experiments (C and D); number of bioprinted constructs (N) = 30 (C), 20 (D), and 10 (E); letters indicate significant differences ($P < 0.05$, Tukey test).

cycle genes and regeneration-related genes are significantly induced (*27*, *28*). Most of these DEGs showed peak expression at day 3, which coincides with most cell divisions (Fig. 2D and fig. S3B). These results suggest that the bioprinted Arabidopsis root cells have the ability to undergo cell divisions and form microcalli.

The division, maintenance, and regeneration of Arabidopsis shoot protoplasts are well established in prior studies (*22*, *29*). To compare our current system with prior data, we bioprinted shoot protoplasts using our bioink optimized for root-derived cells. Similar to root cells, bioprinted shoot cells showed an initial viability of 57.6 ± 4.3% (fig. S4, A and B). After 5 days, the viability was reduced to 20.5 ± 2.2% and further diminished after 7 days (fig. S4A). Although we observed cell divisions as early as 5 days, we did not detect any microcallus formation within the imaged time frame. We hypothesized that the maintenance of cells derived from shoot tissue needs bioink and scaffold materials that are specifically optimized, and

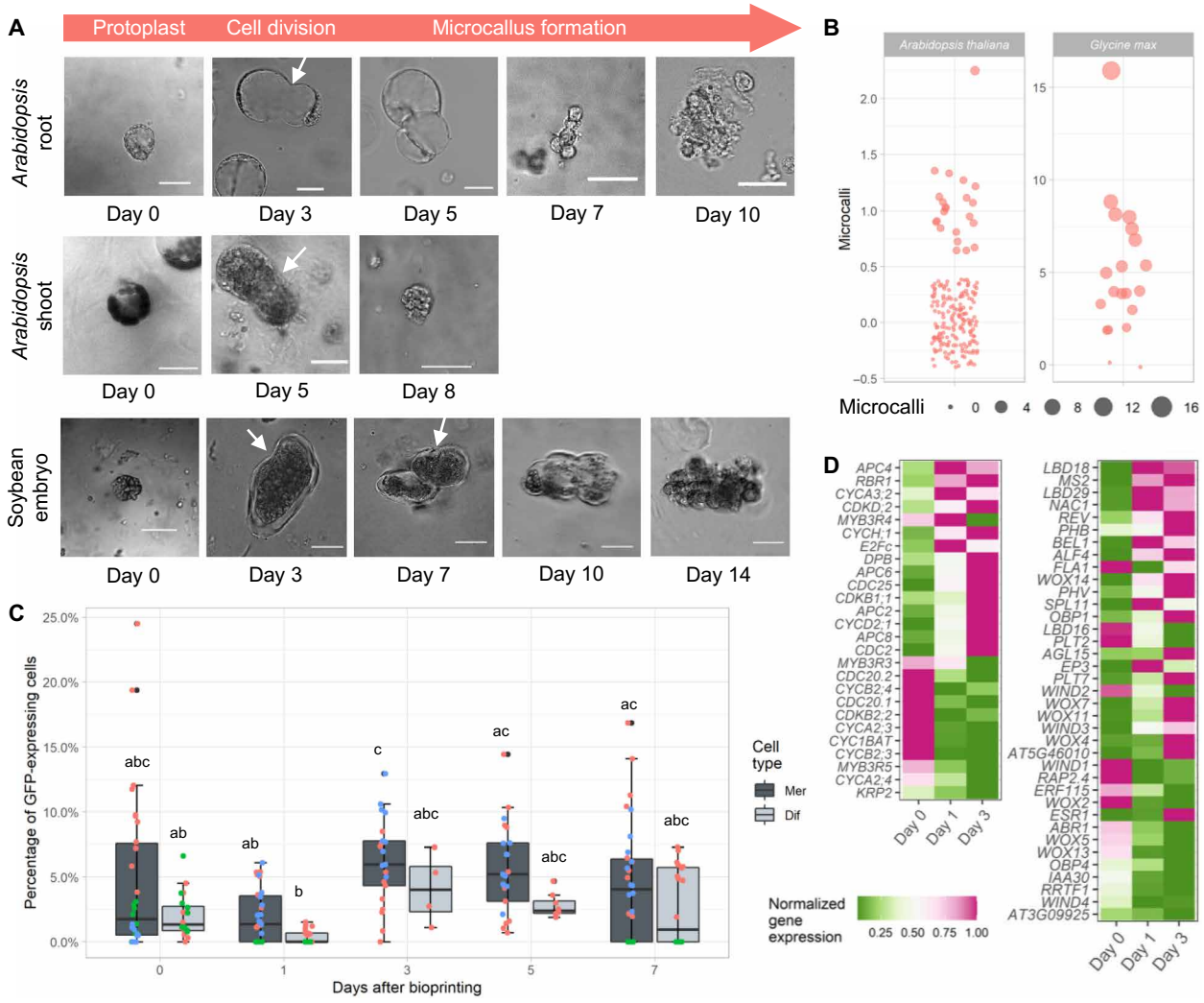

Fig. 2. Cell division and microcallus formation of isolated cells from Arabidopsis roots, shoots, and the shoot meristematic region of the soybean embryonic axis. (**A**) From left to right: High-resolution confocal images of isolated protoplasts, isolated protoplasts undergoing cell division, and microcalli from Arabidopsis roots, shoots, or soybean shoot meristematic regions. Scale bars, 20 μm. (**B**) Number of formed microcalli for Arabidopsis roots and soybean shoot meristematic region. Each dot represents a bioprinted construct. (**C**) Percentage of green fluorescent protein (GFP)–expressing pCYCB1;1:CYCB1;1-GFP meristematic and differentiated root cells on days 0, 1, 3, 5, and 7. Colored dots represent the independent experiments; number of bioprinted constructs (N) = 30; letters indicate significant differences ($P < 0.05$, Tukey test). (**D**) Heatmap of the transcriptional changes for significantly differentially expressed core cell cycle (left) and regeneration (right) genes 0, 1, and 3 days upon bioprinting of differentiated root cells.

repeated the experiment using shoot-optimized bioink (see Materials and Methods) (*21*). After 8 days, we could observe microcalli in 5 of the 10 constructs (Fig. 2A). Thus, specially optimized bioinks might be necessary stimuli for microcallus formation from different tissue types. Similarly, we reasoned that successful 3D bioprinting requires optimized bioinks across species. To demonstrate the extension of bioprinting to crops for studying regeneration, we first optimized a bioink for soybean protoplasts isolated from embryonic shoot meristems (see Materials and Methods) (fig. S4C) (*30*–*37*). In addition, we tailored the bioprinting parameters due to the challenges associated with bioprinting soybean protoplasts. Because the protoplast isolation used a relatively short incubation time in the cell wall digesting enzymes, some tissue was partially digested. To avoid nonuniform extrusion due to nozzle blockages, we used a wider needle (~2×) for bioprinting, which had the added benefit of reducing shear stresses. Using this optimized pipeline, we bioprinted meristematic cells isolated from *Glycine max* (L.) Merr. cv Thorne (*38*) and evaluated cell viability, cell division, and microcallus formation (*39*). Overall, isolated soybean cells showed 28 ± 9.6% viability immediately after bioprinting and 43 ± 11.2% viability after 14 days (fig. S4D). We observed that some cells anisotropically elongate, which correlates with the onset of cell division as early as 3 days after bioprinting. Furthermore, after 14 days, we observed the formation of, on average, five to six microcalli in 90% of the bioprinted constructs (Fig. 2B and data S2). These results indicate that bioprinting can be used as an enabling technology to study cellular regeneration in crops.

Identity maintenance of 3D bioprinting root cells

The root contains multiple cell types, and thus, the bioprinted root cell population is highly heterogeneous. To shed light on the identity of the isolated cells that remain competent for cellular reprogramming leading to regeneration, we examined the cellular identity of our bioprinted root cells and the formed microcalli. To this end, we focused on the ground tissue identity and tracked it using cell type–specific marker lines. Specifically, we used a nuclear-localized transcriptional marker line for the endodermis and cortex endodermis initial (CEI) cells, pEN7:GFP (pENDODERMIS7:GFP), the translational fusion pSCR:SCR-mCherry to identify the endodermis, CEI, and quiescent center (QC), and the enhancer trap J0571 to mark the endodermis and cortex (fig. S2) (*40*). Immediately after bioprinting, we observed between 5.4 ± 1.6% and 10.1 ± 2.2% of meristematic and differentiated protoplasts with EN7 expression, which is comparable to the fractions of endodermal cells in an intact root (table S1). The percentage of EN7-expressing cells increases over time to 25.3 ± 8.7% and 26.3 ± 6.3% on day 5 for meristematic and differentiated root cells, respectively (Fig. 3A). We observed a similar trend with the translational fusion pSCR:SCR-mCherry where the marker's expression increased in both meristematic and differentiated tissues to 54.4 ± 6.5% and 40.7 ± 4.1% on day 7, respectively (Fig. 3, B and C). Overall, we observed an increase in cells expressing the endodermal markers over time, as well as an induction of *EN7* and *SCR* expression in our RNA sequencing (RNA-seq) time course (Fig. 3D). Similarly, published RNA-seq and ATAC-seq (Assay for Transposase-Accessible Chromatin sequencing) data of leaf protoplasts showed an induction of *EN7* and *SCR* expression and chromatin accessibility upon protoplast isolation (*29*). For pEN7:GFP, both meristematic and differentiated bioprinted cells showed an equal fraction of fluorescent cells, while SCARECROW (SCR) expression was significantly increased in meristematic root cells compared to differentiated root cells (Fig. 3B). In addition, we analyzed the enhancer trap line J0571, which includes the additional fluorescence of the cortex (*40*). Similar to pEN7:GFP, J0571-derived protoplasts showed no prominent differences between meristematic and differentiated bioprinted cells (Fig. 3E). Conversely, the percentage of green fluorescent protein (GFP)–expressing cells from J0571 did not increase over time. Overall, the changes in the percentage of cells expressing the endodermal markers indicate that the identity of isolated cells changes over longer periods of time. In line, our RNA-seq showed that several genes required for the initiation or maintenance of the stem cell program are induced within a 3-day window (Figs. 2D and 3D). For example, *CYCLIND6;1* (*CYCD6;1*) was induced at day 1, and SHORTROOT (SHR) and RETINOBLASTOMA-RELATED1 (RBR1) were significantly induced at day 3 (Fig. 3D and data S3). RBR1 binds the SHR-SCR complex to regulate, in coordination with CYCD6;1, the spatial restriction of CEIs' asymmetric divisions (*41*). RBR1, CYCD6;1, and SHR are thus all determinants of ground tissue stem cells and their lineage. Together, the transcriptional induction of these stem cell markers and the changes in cells expressing identity markers suggest that the bioprinted cells gain a stem cell–like identity.

To further gain understanding of the identity of the microcalli, we evaluated whether the formed microcalli showed expression of our marker lines. As such, we could at least partially identify which lineage-specific cells were reprogrammed to pluripotency. Because regenerating cells are very sparse, it is challenging to investigate this process. We only identified sufficient microcalli in the bioprinted constructs of pSCR:SCR-mCherry. Namely, 100% of the pSCR:SCR-mCherry microcalli (seven in total) expressed mCherry fluorescence, which suggested that endodermal, CEI, and/or QC-derived cells were capable of proliferating. In addition, we identified microcalli expressing the pCYCB1;1:CYCB1;1-GFP reporter, the cell cycle marker, to evaluate the microcalli's division potential. Of the pCYCB1;1:CYCB1;1-GFP microcalli, 33% showed GFP fluorescence, which suggests that 3D bioprinted cells are actively dividing.

To show that the microenvironment can be adjusted to evaluate cellular responses to specific conditions, we applied high salinity to the bioprinted constructs and evaluated their viability. Prolonged exposure to such high salinity was shown to induce cell death in Arabidopsis roots, leading to complete growth inhibition (*42*). We used the same experimental conditions and applied them to our bioprinted constructs. To assess the differential cellular response upon high salinity, we tuned the microenvironment after bioprinting. Specifically, we bioprinted isolated meristematic and differentiated pSCR:SCR-mCherry cells using our established protocol. To allow the bioprinted cells to fully acclimate to their environment, we started a high-salinity treatment 2 days after bioprinting by replacing the protoplast induction medium (PIM) refreshment for half of the bioprinted constructs with NaCl-containing PIM (200 mM NaCl). Similarly, as shown by Ambastha *et al.* (*42*), 1 day after treatment, the cell viability decreased significantly. Under salt stress conditions, 43 and 62.1% of the meristematic and differentiated cells, respectively, were viable compared to the control conditions (Fig. 3F). While a 40% reduction of cells expressing SCR upon high salinity was observed in the root (*42*), we did not observe any significant reduction in the number of SCR-expressing cells (fig. S5). Overall, these results show that 3D bioprinting could be used as a tool to determine the influence of stressors on cellular responses.

DISCUSSION

Isolated single cells provide a great system for studying aspects of cell physiology, cell identity, cell-to-cell communication, and cell cycle reentry. Here, we maintained isolated Arabidopsis root cells with high viability for multiple days using a reproducible 3D bioprinting pipeline. Our bioprinting pipeline and the complementary semiautomated image analysis pipeline allowed us to evaluate isolated Arabidopsis cells, including several marker lines, through their developmental lineage. The percentage of isolated cells expressing endodermal markers increases over time, suggesting that the bioprinted cells might be either partially changing identity or transitioning to a previously unknown identity. A previous study in Arabidopsis leaf protoplasts suggests that protoplasts undergo increased stochastic and ectopic gene expression multiple days after isolation (*29*). Thus, an increased ectopic expression might result in the observed changes in expression of identity genes. Another hypothesis is that the loss of an organizational structure, like that of an intact root, leads to non–cell-autonomous signals reaching otherwise unreachable cells or not reaching their intended neighboring cells. This loss and gain of molecular signals and the following disruption in their respective signaling pathways could result in cell identity changes. To further gain insights into these two hypotheses, it would be essential to develop single-cell RNA-seq protocols compatible with encapsulated cells.

Our pipeline allowed us to design the cells' local environment recreating conditions that sustain cell viability and microcallus formation (Fig. 2). Cells isolated from meristematic and differentiated

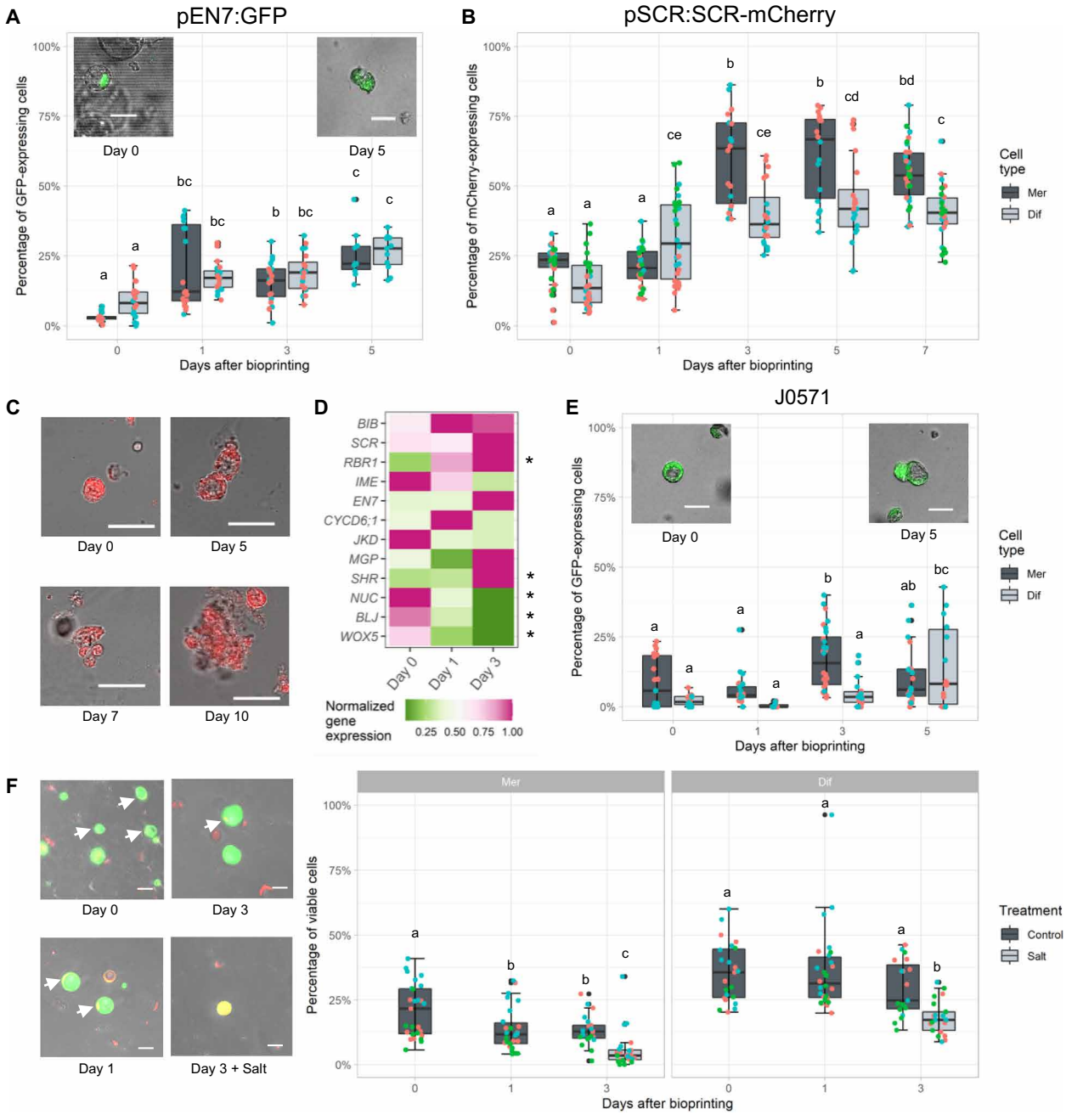

Fig. 3. Ground tissue identity of isolated root cells upon bioprinting. (**A** to **C** and **E**) pEN7:GFP (A), pSCR:SCR-mCherry (B and C), and J0571 (E) bioprinted meristematic and differentiated root cells were imaged on days 0, 1, 3, 5, and 7. Representative high-resolution confocal images of 3D bioprinted cells are given. Scale bars, 20 μm. (**D**) Heatmap of the transcriptional changes for endodermal identity genes on days 0, 1, and 3 upon bioprinting of differentiated root cells. Stars indicate significant DEGs. (**F**) Percentage of viable cells isolated from meristematic (left) and differentiated (right) root cells 0, 1, and 3 days upon bioprinting. High-salinity treatment was performed on day 2. Representative high-resolution confocal images of 3D bioprinted cells are given. Scale bars, 20 μm. Arrows indicate nucleus-located SCR expression. Colored dots represent the independent experiments; number of bioprinted constructs (N) = 20 (A and B) and 30 (C and F); letters indicate significant differences ($P < 0.05$, Tukey test).

Arabidopsis root tissue were able to reenter the cell cycle and form microcalli, indicating a key role for the 3D environment. In line with this hypothesis, preliminary studies in which transgenic *A. thaliana* were cultured within tailored 3D fibrous microenvironments were observed to show growth and morphological characteristics of greater complexity than those cultured on standard 2D scaffolds (*3*). The formed microcalli expressed the endodermal marker SCR. Previous studies showed that callus formation from roots explants was initiated by pericycle cells differentiating into cells resembling root meristems (*16*, *22*). However, the expression of SCR in the bioprinted microcalli indicates that, in addition to pericycle-derived microcallus formation, another reprogramming

mechanism might trigger microcallus formation. The underlying molecular basis of microcallus formation from a single cell is of interest to enhance regeneration of recalcitrant species, increase transformation events, and enable gene editing studies. Using 3D bioprinting to improve single-cell transformation events in combination with gene editing will have potential applications within the agri-biotech field. In this study, we applied our bioprinting pipeline to reprogram meristematic soybean cells to pluripotency. We isolated cells from soybean embryonic axes and were able to show the formation of microcalli after 14 days, a comparable time line with previous studies (*43*). Further identifying structural polymers, signaling molecules, or cell types that generate cell type–specific environments to ensure efficient plant regeneration could have a significant impact in agri-biotech by, for example, accelerating breeding programs.

Our study provides the groundwork for using 3D bioprinting in the plant sciences field and details protocols and guidelines. In addition to the potential applications of 3D bioprinting for studying cell-to-cell communication and plant cell regeneration, 3D bioprinting can be used for researching cellular functions within a tunable environment, including the subcellular and molecular visualization of regulatory proteins, stress-responsive signaling, or cell wall dynamics (*4*). To enable these studies, the identification and detailed classification of the dimension parameters and signaling factors that stimulate plant cell processes, such as proliferation, cell attachment, regeneration, and differentiation, are crucial. Similar as in the mammalian field, 3D bioprinting can be used in the plant field to screen signaling factors and other compounds in a high-throughput manner. Identifying compounds that ensure efficient plant regeneration or other cellular responses could be of interest in a wide range of biotechnological applications. In the future, scaffolds and bioinks based on a variety of synthetic and naturally occurring substrates will need to be designed in a case-by-case manner to engineer specific plant cell–based models and support 3D growth of cells. In addition, external stimuli to induce time-dependent changes in functionality of encapsulated cells may be adopted. Overall, we have shown the potential of 3D bioprinting to study cell viability, cell division, and cellular reprogramming in a tunable microenvironment.

MATERIALS AND METHODS

Plant lines and growth conditions

The following lines were used: wild type, pEN7:GFP (AT4G28100) (*44*), pSCR:SCR-mCherry (AT3G54220) (*45*), and pCYCB1;1:CYCB1;1-GFP (AT4G37490) (*46*) in Columbia-0 background, and J0571 (*40*) in the C24 background. *A. thaliana* seeds were surface-sterilized using 50% bleach and 0.05% Tween 20 for 5 min, followed by a 2-min incubation in 70% ethanol for 2 min. Seeds were rinsed at least seven times with sterile deionized water. Following the last rinse, the seeds were stratified at 4°C for 2 days and plated on 1× Murashige and Skoog agar supplemented with sucrose (1% sucrose total) on top of Nitex mesh (Genesee). All plants were grown in a vertical position at 22°C under long-day conditions (16-hour light/8-hour dark cycle).

Soybean [*G. max* (L.) Merr. cv Thorne] seeds were surface-sterilized using 70% ethanol for 2 min, followed by a 10-min incubation in 50% bleach and 0.05% Tween 20. Seeds were rinsed 10 times in sterile deionized water. Following the last rinse, the seeds were placed in a sterile petri dish, covered with sterile deionized water, and imbibed at 27°C under long-day conditions (16-hour light/8-hour dark cycle) for 24 hours.

Isolation of protoplasts

To avoid contamination, all steps were performed in a laminar flow hood. To prepare the enzyme solution, 0.45 g of cellulase (EMD Millipore) and 0.03 g of pectolyase (Sigma-Aldrich) were dissolved in a 30-ml solution containing 5.465 g of mannitol, 0.05 g of 0.01% bovine serum albumin, 500 μl of 0.2 M magnesium chloride, 500 μl of 0.2 M calcium chloride, 500 μl of 1 M MES, 500 μl of 1 M potassium chloride, 50 ml of deionized water, and tris-HCl (pH 5.5). The enzyme solution was sterilized using a 0.20-μm syringe filter. For each sample, 7 ml of fresh enzyme solution was pipetted into 35-mm-diameter petri dishes. We avoided creating bubbles when pipetting the enzyme solution to avoid cell lysis at later stages in the protocol.

A 70-μm cell strainer was placed in each 35-mm-diameter petri dish. Approximately 1 to 2 mm of the root tip were cut to isolate the meristematic region of the root and put into the strainer in enzyme solution. The samples were incubated for 2 hours at 85 rpm at room temperature with supplemental stirring every 30 min. Next, all of the cells and enzyme solution were transferred to a 15-ml conical tube and centrifuged for 6 min at 200*g*. The supernatant was removed, and the pellet was resuspended with 100 μl of PIM or protoplast callus induction medium (PCIM) for the shoot-derived cells (*47*, *48*). PIM (*A. thaliana*) contains a cocktail of growth hormones, sugar, mannitol to ensure a proper osmolarity, folic acid (*18*, *19*), and PSK (*17*, *49*) (Table 1). The resuspended solution was transferred to a 70-μm filter placed on top of a 50-ml conical tube. Another 100 μl of PIM was filtered through to collect any leftover cells stuck on the 70-μm filter. All the filtered liquid was transferred to a 40-μm filter placed on top of a 50-ml conical tube. The subsequent filtered liquid contains the protoplasts used for bioprinting. The volume of cells in each solution was estimated using a hemocytometer. The starting cell densities are listed in Table 2.

For soybean protoplast isolation, 2% (w/v) cellulase (EMD Millipore) and 0.03% (w/v) pectolyase (Sigma-Aldrich) were dissolved in a 30-ml solution containing 13% mannitol, KH_2PO_4 (27.2 mg/liter), KNO_3 (100 mg/liter), calcium chloride (150 mg/liter), magnesium chloride (250 mg/liter), iron(III) sulfate (2.5 mg/liter), KI (0.16 mg/liter), 50 ml of deionized water, and tris-HCl (pH 5.5). The enzyme was sterilized using a 0.20-μm syringe filter. For each sample, 7 ml of fresh enzyme solution was pipetted into 35-mm-diameter petri dishes. We avoided creating bubbles when pipetting the enzyme solution to avoid cell lysis at later stages in the protocol.

A 70-μm cell strainer was placed in each 35-mm-diameter petri dish. Meristematic shoot tissue from the embryonic axis from imbibed soybean seeds was isolated and put into the strainer in enzyme solution. The samples were incubated for 2 hours at 85 rpm at room temperature with supplemental stirring every 30 min. Next, all of the cells and enzyme solution were transferred to a 15-ml conical tube and centrifuged for 6 min at 200*g*. The supernatant was removed, and the pellet was resuspended with 1 ml of bioink (Table 1). The resuspended solution was transferred to a 70-μm filter placed on top of a 50-ml conical tube. All the filtered liquid was transferred to a 40-μm filter placed on top of a 50-ml conical tube. The subsequent filtered liquid contains the protoplasts used for bioprinting. The volume of cells in each solution was estimated using a hemocytometer.

Bioink and 3D bioprinter

The isolated protoplasts were resuspended in a specialized bioink that consisted of the PIM that was supplemented with 0.6% low melting agarose (Sigma-Aldrich) to provide support for cell growth.

Table 1. Recipe for PIM, SIM, and PCIM. The pH was set to 5.7 followed by autoclaving. Antibiotics were filter-sterilized and added after autoclaving. PIM, protoplast induction medium; SIM, shoot induction medium; PCIM, protoplast callus induction medium [adopted from Sakamoto *et al.* (*21*)].

		PIM (*A. thaliana*)	PIM (soybean)	SIM (soybean)	PCIM (*A. thaliana*)
		in 100 ml of H_2O	in 100 ml of H_2O	in 100 ml of H_2O	in 100 ml of H_2O
$^1/_2$ B5 medium	Sigma-Aldrich	0.153 g	0.153 g	0.32 g	0.153 g
Sucrose	Thermo Fisher Scientific	10.3 g	2 g	3 g	/
Glucose	Sigma-Aldrich	/	/	/	2 g
D-Mannitol	Sigma-Aldrich	/	7.28 g	/	7.28 g
2,4-D (2,4-Dichlorophenoxyacetic acid)	MP Biomedicals	0.02 mg	/	/	0.1 mg
NAA (1-Naphthaleneacetic acid)	Sigma-Aldrich	/	0.1 mg	/	/
BAP (6-Benzylaminopurine)	MP Biomedicals	0.03 mg	0.01 mg	0.11 mg	/
TDZ (Thidizuron)	Caisson Labs	/	/	/	17.6 µg
MES	Thermo Fisher Scientific	0.01 g	/	0.059 g	0.05 g
$CaCl_2$-H_2O_2	VWR	37.5 mg	/	/	/
Sodium succinate	Sigma-Aldrich	27 mg	/	/	/
Folic acid	Sigma-Aldrich	0.2 mg	/	/	/
Phytosulfokine	MyBioSource	0.0085 mg	/	/	/
Timentin	VWR	2 mg	2 mg	5 mg	2 mg
Cefotaxime	Caisson Labs	/	/	20 mg	/
Vancomycin	Research Products International	/	/	5 mg	/

Table 2. 3D bioprinting parameters.

Parameter	*Arabidopsis*	Soybean
Inner diameter needle tip	159 µm (30 gauge)	413 µm (22 gauge)
Extrusion pressure	20 kPa	20 kPa
Printhead	Extrusion	Extrusion
Extrusion temperature	37°C	37°C
Extrusion time	0.8 s	0.8 s
Printbed temperature	Room temperature or 15°C	Room temperature
Average cellular density	1392 ± 152 cells/µl	1379 ± 288 cells/µl

Namely, the PIM containing the protoplasts was mixed with a stock scaffold solution consisting of 2.4% agarose dissolved in PIM, at a ratio of 3:1, to yield the desired bioink used for bioprinting. For the experiments using alginate as scaffold material, the PIM or PCIM containing the protoplasts was mixed with a stock solution of 3% alginate dissolved in PIM or PCIM, respectively, at a ratio of 3:1.

The protoplasts were printed with a 3-ml syringe barrel that incorporated an axial piston, using an extrusion 3D bioprinter (CELLINK BIO X), into an eight-well µ-slide (ibidi), which facilitated the acquisition of cell images at multiple time points. To facilitate the collection of the bioprinted constructs for transcriptomics, the protoplasts were printed into a two-well µ-slide (ibidi). The bioink-embedded protoplasts are printed at a temperature of 37°C, rendering liquid low melting agarose. To minimize the effects of shear stress on the suspended cells during the 3D bioprinting process, the sterile blunt needle tip inner diameter and extrusion pressure were optimized. The optimized bioprinting parameters used are listed in Table 2. The extrusion of the protoplast-embedded bioink was followed by reversible thermal gelation of the agar by free convection, which resulted in a temperature reduction and solidification of the scaffold material, thus ensuring the fabrication of the desired 3D construct. The gelation of the alginate constructs in each well was achieved by a short treatment with 1% $CaCl_2$ for 30 s. The protoplast-embedded bioink was extruded into eight-well µ-slides, with each well holding four bioprinted droplets. To prevent drying of the 3D constructs and allow for nutrient and hormone exchange, the cells are covered with 250 µl of PIM in each well. Resupplantation of the PIM was performed every 2 days. The bioprinted constructs were kept in the dark. For soybean bioprinted constructs, 250 µl of shoot induction medium was used as refreshment at 7 and 14 days after bioprinting.

Staining and confocal imaging

Before image acquisition, cells were stained with 0.01% fluorescein diacetate (Sigma-Aldrich), a cell-permeable esterase substrate that measures intracellular enzymatic activity. For fig. S1, cells were also stained with 1 µM propidium iodide. Image acquisition was performed on a Zeiss LSM 880 confocal microscope. For each independent experiment, 10 bioprinted constructs were imaged by obtaining z-stack images with 5 to 20 µm slices. Each z-stack contained between 50 and 300 cells. The obtained microscopy images were sorted per day, and each folder of images corresponding to a specific day was analyzed separately with our in-house developed pipeline to improve counting strategies.

Automated image analysis pipeline

To facilitate repeatable, robust, and rapid analysis of a large number of confocal images of cells, we generated an automated open source image analysis pipeline that can be run through an R Shiny GUI (*50*). The GUI runs three in-house developed python scripts in the back end. The first python script separates the fluorescence and bright-field channels, performs a *z*-projection of the bright-field channel using minimum intensity, and saves the projections as .png files. This function relies on the pyimageJ package (*51*). The second python script quantifies cells in the bright-field channel using the publicly available OpenCV Computer vision library for tracking and counting of cells. The script performs contrast-limited adaptive histogram equalization on the bright-field images and uses an edge detection algorithm to detect and count cells (*52*). The third script separates fluorescence and bright-field channels, performs *z*-projection of the fluorescence channel using maximum intensity, and detects and quantifies cells in the fluorescent channels with ComDet v 0.5.3, an open source plugin for ImageJ (*53*). This function also relies on the pyimageJ package (*51*). The program code for the entire image analysis pipeline contained in Python and further developed into an R Shiny application (*50*) can be easily accessed, along with the usage instructions, from the Github repository at https://github.com/LisaVdB/Confocal-z-stack-cell-detection or Zenodo at 10.5281/zenodo.7012765.

To run our shiny R GUI, the required dependencies need to be installed. We recommend using anaconda to set up the environment, which includes R (4.1.2), RStudio, python (3.8.12), OpenCV (4.5.4), pyimageJ (1.0.2), and JAVA jdk (11.0.9.1). More instructions on creating the correct environment can be found on the Github repository. Next, download and unzip the Github repository. To successfully run the GUI, the python path in the .Rprofile needs to be changed to the python path of the setup environment. Copy the to-analyze confocal lsm images in the "in" folder. To launch the GUI, open the "server" or "ui" file in Rstudio and click on "Run App" on the bar menu. The GUI will launch in your browser or within Rstudio depending on your settings. Adjust the parameters with the sliders to analyze the fluorescent and bright-field channels of the confocal images as follows. For the bright-field channel analysis, the minimum and maximum area determine the size of the detected cells. The threshold values are used to convert the .png images into multiple binary images, one for each threshold ranging from the minimum to the maximum threshold with a step of 2. Thus, pixels below the minimum and above the maximum threshold will always be 0, while the rest is set to 255. Pick a small minimum threshold and adjust it such that there are little to zero false-positive and false-negative detected cells. The circularity parameter defines how circular the cells are. The maximum circularity is 1 and describes a perfect circle. The convexity characterizes the shape of the cells to be detected. The more circular the cells are, the higher their convexity is. The color parameter filters can be set either to 0 or 1 to detect dark or light cells, respectively. For the fluorescent channels, the area and threshold parameters can be set from 0 to a certain value to determine the area of the detected cells or the intensity difference between the foreground and background of the binary images, respectively. The options "include large cells" and "split large cells" are marked when it is necessary to quantify large particles and further split them into smaller ones, respectively. After the completion of the image analysis, the cell counts can be downloaded as a .csv file, and output images can be found in the "out," "bf," and "gc" folders. The cell counts were processed and visualized in R (version 4.0.2) using ggplot2 (*54*).

Transcriptomics

For the expression profiles, we collected RNA from bioprinted constructs and isolated cells from meristematic and differentiated root tissue as follows. The liquid PIM was removed from the two-well slides without disturbing the bioprinted constructs. Next, bioprinted constructs were collected in a 2-ml Eppendorf tube with 0.5-mm glass beads (Next Advance) using a 1000-ml pipette tip and immediately flash-frozen in liquid nitrogen. In addition, isolated cells before bioprinting were also collected in a 2-ml Eppendorf tube with 0.5-mm glass beads (Next Advance) and immediately flash-frozen in liquid nitrogen. We performed three independent experiments. To extract the RNA, 500 µl of TRIzol (Thermo Fisher Scientific) was added and the cells were disrupted within TRIzol using a mill mixer at 30 Hz for 5 min at room temperature. RNA was further purified using chloroform and the RNeasy Micro Kit (Qiagen). cDNA synthesis and amplification were performed using the NEBNext Poly(A) mRNA Magnetic Isolation Module followed by the NEBNext Ultra II Directional RNA Library Prep and NEBNext Multiplex Oligos for Illumina (Dual Index Primers Set 1) and sequenced using an Illumina NovaSeq6000 sequencing machine, with 150–base pair paired-end reads.

Gene expression analysis of raw RNA-seq data was performed using the TuxNet interface (*55*). Specifically, TuxNet uses ea-utils fastq-mcf for preprocessing, hisat2 for genome alignment, and Cufflinks for differential expression analysis (data S4). The expression was scaled for each gene using a min-max scaler formula, where the minimum and the maximum were set to 0 and 1, respectively. Significant DEGs were selected using a *q* value threshold of 0.05 and an absolute fold change threshold of 2 of the pairwise comparisons between the three time points in bioprinted differentiated root cells and between the bioprinted constructs and the isolated cells at day 0. Selected DEGs were clustered using hierarchical clustering. Enriched GO terms for each cluster were identified with PANTHER (*56*). To summarize and reduce redundant GO terms, Revigo was used (*57*). When comparing bioprinted constructs with isolated cells from meristematic and differentiated tissue at day 0, we identified 1428 and 1514 DEGs, respectively (fig. S6A). We further identified six clusters of coexpressed genes for the combined 2463 DEGs that showed different enriched GO terms (fig. S6B). The largest cluster 1 and cluster 6 contain genes up-regulated in the isolated cells of which the enriched GO terms relate to metabolic processes. Clusters 2, 3, and 4 contain genes up-regulated in the bioprinted constructs of which the enriched GO terms relate to protein folding and RNA transport.

Specific cell cycle or regeneration genes were selected by a keyword search in The Arabidopsis Information Resource (TAIR) of genes associated with either "regeneration," "redifferentiation," "dedifferentiation," or "mitotic cell cycle." Additional cell differentiation- and regeneration-related genes were identified from callus regeneration studies (*1*, *28*). To visualize gene expression, heatmaps of the scaled expression were generated in R (version 4.0.2) using ggplot2 (*54*). All sequencing data are available at Gene Expression Omnibus (GEO) (GSE208176).

SUPPLEMENTARY MATERIALS

Supplementary material for this article is available at https://science.org/doi/10.1126/sciadv.abp9906

REFERENCES AND NOTES

1. M. Ikeuchi, Y. Ogawa, A. Iwase, K. Sugimoto, Plant regeneration: Cellular origins and molecular mechanisms. *Development* **143**, 1442–1451 (2016).

2. K. Duval, H. Grover, L.-H. Han, Y. Mou, A. F. Pegoraro, J. Fredberg, Z. Chen, Modeling physiological events in 2D vs. 3D cell culture. *Physiology* **32**, 266–277 (2017).
3. Y. Luo, A. Lode, A. R. Akkineni, M. Gelinsky, Concentrated gelatin/alginate composites for fabrication of predesigned scaffolds with a favorable cell response by 3D plotting. *R. Soc. Chem. Adv.* **5**, 43480–43488 (2015).
4. S. Mehrotra, S. Kumar, V. Srivastava, T. Mishra, B. N. Mishra, 3D bioprinting in plant science: An interdisciplinary approach. *Trends Plant Sci.* **25**, 9–13 (2020).
5. R. Wightman, C. J. Luo, From mammalian tissue engineering to 3D plant cell culture. *Biochemist* **38**, 32–35 (2016).
6. I. Chiesa, C. De Maria, A. Lapomarda, G. M. Fortunato, F. Montemurro, R. Di Gesù, R. S. Tuan, G. Vozzi, R. Gottardi, Endothelial cells support osteogenesis in an in vitro vascularized bone model developed by 3D bioprinting. *Biofabrication* **12**, 025013 (2020).
7. C. S. Ong, P. Yesantharao, C. Y. Huang, G. Mattson, J. Boktor, T. Fukunishi, H. Zhang, N. Hibino, 3D bioprinting using stem cells. *Pediatric Res.* **83**, 223–231 (2018).
8. X. Ma, J. Liu, W. Zhu, M. Tang, N. Lawrence, C. Yu, M. Gou, S. Chen, 3D bioprinting of functional tissue models for personalized drug screening and in vitro disease modeling. *Adv. Drug Deliv. Rev.* **132**, 235–251 (2018).
9. E. Maloney, C. Clark, H. Sivakumar, K. Yoo, J. Aleman, S. A. P. Rajan, S. Forsythe, A. Mazzocchi, A. W. Laxton, S. B. Tatter, R. E. Strowd, K. I. Votanopoulos, A. Skardal, Immersion bioprinting of tumor organoids in multi-well plates for increasing chemotherapy screening throughput. *Micromachines (Basel)* **11**, 208 (2020).
10. J. Xu, H. Hofhuis, R. Heidstra, M. Sauer, J. Friml, B. Scheres, A molecular framework for plant regeneration. *Science* **311**, 385–388 (2006).
11. M. Guvendiren, J. Molde, R. M. D. Soares, J. Kohn, Designing biomaterials for 3D printing. *ACS Biomater Sci. Eng.* **2**, 1679–1693 (2016).
12. F. Pampaloni, E. G. Reynaud, E. H. K. Stelzer, The third dimension bridges the gap between cell culture and live tissue. *Nat. Rev. Mol. Cell Biol.* **8**, 839–845 (2007).
13. M. J. Bissell, A. Rizki, I. S. Mian, Tissue architecture: The ultimate regulator of breast epithelial function. *Curr. Opin. Cell Biol.* **15**, 753–762 (2003).
14. J. A. Hickman, R. Graeser, R. de Hoogt, S. Vidic, C. Brito, M. Gutekunst, H. van der Kuip; IMI PREDECT Consortium, Three-dimensional models of cancer for pharmacology and cancer cell biology: Capturing tumor complexity in vitro/ex vivo. *Biotechnol. J.* **9**, 1115–1128 (2014).
15. H. Gudapati, M. Dey, I. Ozbolat, A comprehensive review on droplet-based bioprinting: Past, present and future. *Biomaterials* **102**, 20–42 (2016).
16. T. Pasternak, I. A. Paponov, S. Kondratenko, Optimizing protocols for arabidopsis shoot and root protoplast cultivation. *Plants* **10**, 375 (2021).
17. S. Ochatt, C. Conreux, R. M. Mcolo, G. Despierre, J.-B. Magnin-Robert, B. Raffiot, Phytosulfokine-alpha, an enhancer of in vitro regeneration competence in recalcitrant legumes. *Plant Cell Tiss. Org. Cult.* **135**, 189–201 (2018).
18. M. Benmoussa, S. Mukhopadhyay, Y. Desjardins, Factors influencing regeneration from protoplasts of Asparagus densiflorus cv. Sprengeri. *Plant Cell Rep.* **17**, 123–128 (1997).
19. H. Aoyagi, H. Tanaka, Measurement of viable plant cell and protoplast concentrations with specialized fluorometer. *J. Ferment. Bioeng.* **77**, 517–521 (1994).
20. G. R. López-Marcial, A. Y. Zeng, C. Osuna, J. Dennis, J. M. García, G. D. O'Connell, Agarose-based hydrogels as suitable bioprinting materials for tissue engineering. *ACS Biomater Sci. Eng.* **4**, 3610–3616 (2018).
21. Y. Sakamoto, A. Kawamura, T. Suzuki, S. Segami, M. Maeshima, S. Polyn, L. De Veylder, K. Sugimoto, Transcriptional activation of auxin biosynthesis drives developmental reprogramming of differentiated cells. *Plant Cell* koac218 (2022).
22. K. Sugimoto, Y. Jiao, E. M. Meyerowitz, Arabidopsis regeneration from multiple tissues occurs via a root development pathway. *Development Cell* **18**, 463–471 (2010).
23. A. Dodero, L. Pianella, S. Vicini, M. Alloisio, M. Ottonelli, M. Castellano, Alginate-based hydrogels prepared via ionic gelation: An experimental design approach to predict the crosslinking degree. *Eur. Polym. J.* **118**, 586–594 (2019).
24. K.-A. Leslie, R. Doane-Solomon, S. Arora, S. J. Curley, C. Szczepanski, M. M. Driscoll, Gel rupture during dynamic swelling. *Soft Matter* **17**, 1513–1520 (2021).
25. E. A. Growney Kalaf, R. Flores, J. G. Bledsoe, S. A. Sell, Characterization of slow-gelling alginate hydrogels for intervertebral disc tissue-engineering applications. *Mater. Sci. Eng. C* **63**, 198–210 (2016).
26. A. Schnittger, L. De Veylder, The dual face of cyclin B1. *Trends Plant Science* **23**, 475–478 (2018).
27. M. Ikeuchi, M. Shibata, B. Rymen, A. Iwase, A.-M. Bågman, L. Watt, D. Coleman, D. S. Favero, T. Takahashi, S. E. Ahnert, S. M. Brady, K. Sugimoto, A gene regulatory network for cellular reprogramming in plant regeneration. *Plant Cell Physiol.* **59**, 765–777 (2018).
28. M. Ikeuchi, K. Sugimoto, A. Iwase, Plant callus: Mechanisms of induction and repression. *Plant Cell* **25**, 3159–3173 (2013).
29. M. Xu, Q. Du, C. Tian, Y. Wang, Y. Jiao, Stochastic gene expression drives mesophyll protoplast regeneration. *Sci. Adv.* **7**, eabg8466.
30. C. N. Stewart Jr., M. J. Adang, J. N. All, H. R. Boerma, G. Cardineau, D. Tucker, W. A. Parrott, Genetic transformation, recovery, and characterization of fertile soybean transgenic for a synthetic Bacillus thuringiensis crylAc gene. *Plant Physiol.* **112**, 121–129 (1996).
31. J. J. Finer, M. D. McMullen, Transformation of soybean via particle bombardment of embryogenic suspension culture tissue. *In Vitro Cell Dev. Biol. Plant* **27**, 175–182 (1991).
32. A. Droste, G. Pasquali, M. H. Bodanese-Zanettini, Transgenic fertile plants of soybean [*Glycine max* (L.) Merrill] obtained from bombarded embryogenic tissue. *Euphytica* **127**, 367–376 (2002).
33. C. M. Hernandez-Garcia, A. P. Martinelli, R. A. Bouchard, J. J. Finer, A soybean (*Glycine max*) polyubiquitin promoter gives strong constitutive expression in transgenic soybean. *Plant Cell Rep.* **28**, 837–849 (2009).
34. B. Wiebke-Strohm, A. Droste, G. Pasquali, M. B. Osorio, L. Bücker-Neto, L. M. P. Passaglia, M. Bencke, M. S. Homrich, M. Margis-Pinheiro, M. H. Bodanese-Zanettini, Transgenic fertile soybean plants derived from somatic embryos transformed via the combined DNA-free particle bombardment and *Agrobacterium* system. *Euphytica* **177**, 343–354 (2011).
35. M. S. Homrich, L. M. P. Passaglia, J. F. Pereira, P. F. Bertagnolli, G. Pasquali, M. A. Zaidi, I. Altosaar, M. H. Bodanese-Zanettini, Resistance to anticarsia gemmatalis Hübner (Lepidoptera, Noctuidae) in transgenic soybean (*Glycine max* (L.) Merrill Fabales, Fabaceae) cultivar IAS5 expressing a modified Cry1Ac endotoxin. *Genet. Mol. Biol.* **31**, 522–531 (2008).
36. M. S. Homrich, B. Wiebke-Strohm, R. L. M. Weber, M. H. Bodanese-Zanettini, Soybean genetic transformation: A valuable tool for the functional study of genes and the production of agronomically improved plants. *Genet. Mol. Biol.* **35**, 998–1010 (2012).
37. C. Wu, J. M. Chiera, P. P. Ling, J. J. Finer, Isoxaflutole treatment leads to reversible tissue bleaching and allows for more effective detection of GFP in transgenic soybean tissues. *In Vitro Cell Dev. Biol. Plant* **44**, 540–547 (2008).
38. B. A. McBlain, R. J. Fioritto, S. K. S. Martin, A. J. Calip-Dubois, A. F. Schmitthenner, R. L. Cooper, R. J. Martin, Registration of "Thorne" soybean. *Crop. Sci.* **33**, 1406 (1993).
39. W. Lin, J. T. Odell, R. M. Schreiner, Soybean protoplast culture and direct gene uptake and expression by cultured soybean protoplasts. *Plant Physiol.* **84**, 856–861 (1987).
40. J. Haseloff, E. L. Dormand, A. H. Brand, Live imaging with green fluorescent protein. *Methods Mol. Biol.* **122**, 241–259 (1999).
41. A. Cruz-Ramírez, S. Díaz-Triviño, I. Blilou, V. A. Grieneisen, R. Sozzani, C. Zamioudis, P. Miskolczi, J. Nieuwland, R. Benjamins, P. Dhonukshe, J. Caballero-Pérez, B. Horvath, Y. Long, A. P. Mähönen, H. Zhang, J. Xu, J. A. Murray, P. N. Benfey, L. Bako, A. F. Marée, B. Scheres, A bistable circuit involving SCARECROW-RETINOBLASTOMA integrates cues to inform asymmetric stem cell division. *Cell* **150**, 1002–1015 (2012).
42. V. Ambastha, Y. Friedmann, Y. Leshem, Laterals take it better—Emerging and young lateral roots survive lethal salinity longer than the primary root in Arabidopsis. *Sci. Rep.* **10**, 3291 (2020).
43. S. K. Dhir, S. Dhir, J. M. Widholm, Regeneration of fertile plants from protoplasts of soybean (*Glycine max* L. Merr.): Genotypic differences in culture response. *Plant Cell Rep.* **11**, 285–289 (1992).
44. R. Heidstra, D. Welch, B. Scheres, Mosaic analyses using marked activation and deletion clones dissect Arabidopsis SCARECROW action in asymmetric cell division. *Genes Dev.* **18**, 1964–1969 (2004).
45. N. M. Clark, E. Hinde, C. M. Winter, A. P. Fisher, G. Crosti, I. Blilou, E. Gratton, P. N. Benfey, R. Sozzani, Tracking transcription factor mobility and interaction in Arabidopsis roots with fluorescence correlation spectroscopy. *eLife* **5**, e14770 (2016).
46. E. Buckner, I. Madison, H. Chou, A. Matthiadis, C. E. Melvin, R. Sozzani, C. Williams, T. A. Long, Automated imaging, tracking, and analytics pipeline for differentiating environmental effects on root meristematic cell division. *Front. Plant Sci.* **10**, 1487 (2019).
47. J. Park, S. Choi, S. Park, J. Yoon, A. Y. Park, S. Choe, DNA-free genome editing via ribonucleoprotein (RNP) delivery of CRISPR/Cas in lettuce. *Methods Mol. Biol.* **1917**, 337–354 (2019).
48. J. Park, S. Choe, DNA-free genome editing with preassembled CRISPR/Cas9 ribonucleoproteins in plants. *Transgenic Res.* **28**, 61–64 (2019).
49. A. Kiełkowska, A. Adamus, Peptide growth factor phytosulfokine-α stimulates cell divisions and enhances regeneration from *B. oleracea* var. *capitata* L. protoplast culture. *J. Plant Growth Regul.* **38**, 931–944 (2019).
50. W. Chang, J. Cheng, J. J. Allaire, C. Sievert, B. Schloerke, Y. Xie, J. Allen, J. McPherson, A. Dipert, B. Borges, shiny: Web application framework for R (2021); https://CRAN.R-project.org/package=shiny.
51. C. Rueden, E. Evans, L. Yang, M. Pinkert, Y. Liu, M. Hiner, J. Eglinger, H. Mary, Macarse, D. Hereñú, P. Hanslovsky, W. Ouyang, imagej/pyimagej: v1.0.2 (2021); https://zenodo.org/record/5537065.
52. G. Bradski, The openCV library. *Dr. Dobb's J. Softw. Tools Prof. Program.* **25**, 120–123 (2000).
53. E. Katrukha, ComDet plugin for ImageJ (2020).
54. H. Wickham, ggplot2: Elegant Graphics for Data Analysis (Springer-Verlag New York, 2016).

55. R. J. Spurney, L. Van den Broeck, N. M. Clark, A. P. Fisher, M. A. de Luis Balaguer, R. Sozzani, Tuxnet: A simple interface to process RNA sequencing data and infer gene regulatory networks. *Plant J.* **101**, 716–730 (2020).
56. H. Mi, D. Ebert, A. Muruganujan, C. Mills, L.-P. Albou, T. Mushayamaha, P. D. Thomas, PANTHER version 16: A revised family classification, tree-based classification tool, enhancer regions and extensive API. *Nucleic Acids Res.* **49**, D394–D403 (2021).
57. F. Supek, M. Bošnjak, N. Škunca, T. Šmuc, REVIGO summarizes and visualizes long lists of gene ontology terms. *PLOS ONE* **6**, e21800 (2011).

Acknowledgments: We thank the Cellular and Molecular Imaging Facility (CMIF) at the North Carolina (NC) State University, specifically M. Zareba and E. Johannes, for imaging advice. We thank the NC State University Genomic Sciences Laboratory (GSL) (Raleigh, NC, USA) for prompt sequencing advice. We thank coffee, sharp blades, petri dishes, and functional cellulase.
Funding: This study was supported by National Science Foundation (NSF) EAGER MCB no. 203928 (T.H. and R.S.) and BASF Plant Sciences (T.H. and R.S.). **Author contributions:** Conceptualization: L.V.d.B., M.F.S., S.K., R.S., and T.H. Formal analysis: L.V.d.B. Funding acquisition: R.S. and T.H. Investigation: L.V.d.B., M.F.S., S.K., R.J.S., M.A.T., C.M., M.G., R.P., A.M., I.M., T.N., and A.H. Methodology: L.V.d.B., M.F.S., S.K., R.S., T.H., B.L., and M.S. Software: L.V.d.B., S.K., M.A.T., and R.J.S. Supervision: R.S. Writing—original draft: L.V.d.B., M.F.S., and S.K. Writing—review and editing: L.V.d.B., M.F.S., S.K., R.S., and B.L. **Competing interests:** R.S. and T.H. disclose a submitted patent application (PCT/US2021/023398). All other authors declare no competing interest. **Data and materials availability:** All data needed to evaluate the conclusions in the paper are present in the paper and/or the Supplementary Materials. Scripts for our high-throughput and automatic image analysis are available at https://github.com/LisaVdB/Confocal-z-stack-cell-detection and 10.5281/zenodo.7012765. All sequencing data are available at GEO (GSE208176).

Submitted 10 March 2022
Accepted 25 August 2022
Published 14 October 2022
10.1126/sciadv.abp9906